# Investigation of near optimum iterative equalizers and decoders for optical coherent Gbit/s transmission

Klaus Oestreich, Joachim Speidel

Universität Stuttgart, Institut für Nachrichtenübertragung, 70569 Stuttgart
E-Mail: klaus.oestreich@inue.uni-stuttgart.de

## Abstract

We investigate a receiver for coherent optical communication with QPSK modulated signals. The receiver consists of a BCJR equalizer and LDPC decoding which are arranged as a turbo equalizer. Target is to find dedicated LDPC codes with overhead of about 7% to 14%. It turns out, that an LDPC code with overhead $O_c = 12.5\%$ and codeword length $N = 9198$ is most suitable with respect to performance, complexity and overhead. Furthermore the performance of the receiver is compared to a simpler receiver which compensates chromatic dispersion by the use of FIR filters. The comparison shows a gain of the turbo equalizer of up to 2.5 dB.

## 1 Introduction

The manifold of todays internet applications as well as digital television with HDTV place a demand to ever increasing bitrates in optical communication systems. Thus, the trend in the research area in the last years is coherent optical detection associated with digital signal processing for long haul networks with bitrates of 100 Gbit/s and beyond [1], [2]. Linear impairments like chromatic dispersion (CD) and polarization mode dispersion (PMD) can be compensated with linear filters [3], [4]. On the one hand, these receivers have a moderate complexity. On the other hand their performance is not optimal.

A near optimum approach is low-density parity-check (LDPC) coded turbo equalization. Turbo equalization [5], [6] as a combination of equalization and decoding is widely discussed for mobile communications. For intensity modulated transmission over an optical link turbo equalization in combination with the BCJR equalizer for detection and an LDPC soft-in soft-out (SISO) decoder for forward error correction (FEC) has been investigated. It has been shown, that such a receiver can reach the rate-distortion limit with only a small gap [7], [8], [9].

These results motivate the investigations in this paper to apply such schemes to optical coherent systems. We present a solution how to adapt the BCJR algorithm to quadrature phase shift keying (QPSK) modulated signals and how to incorporate a priori information of symbols. Furthermore we will present an efficient way to estimate the probability density functions (PDFs) required for equalization based on collected histograms.

For coherent optical transmission LDPC codes with high code rate are preferred, as they do not extend the signal bandwidth aggressively. Thus we present suitable codes with overhead between 6.7% to 14.3%. As a requirement, these codes have to offer a good compromise between high error correction performance and complexity. Therefore we present an estimation of the complexity of the decoder depending on the LDPC parameters and the performance of several promising codes.

This paper is organized as follows. In section 2 the model of the coherent optical system with turbo equalization is introduced. The two main parts of the turbo equalizer, the BCJR detector and the LDPC decoder, are explained in section 3. Simulation results are given in section 4, and section 5 concludes the paper.

## 2 System Model

We consider the coherent optical system of **Fig. 1**. The basic elements are the transmitter (TX), the standard single mode fiber (SSMF) and the optically preamplified receiver (RX) comprising the turbo equalizer.

The information bits $b_k$ to be transmitted have the bit rate $R_b = 40$ Gb/s. For FEC at the receiver, the LDPC encoder adds redundancy to the information bits. Thus the rate of the binary symbols $a_m$ is enlarged by factor $R_c^{-1}$ which is the reciprocal code rate. The binary symbols are fed into a time domain raised cosine impulse shaper with roll-off factor 0.35 for non-return-to-zero (NRZ) impulse generation. Finally an optical QPSK modulator (QM) consisting of two Mach-Zehnder modulators (MZM) provides the optical tx-signal.

The symbol rate on the fiber is

$$R_s = \frac{R_b}{M \cdot R_c}, \tag{1}$$

with $M = 2$ as a 4-ary modulation scheme is used. Along the fiber the optical signal is affected by CD, PMD and attenuation. An erbium doped fiber amplifier (EDFA) at the receiver side with amplification factor $G$ completely compensates the loss of the fiber. This amplifier is the major source of noise in the transmission system. The noise is modeled by an amplified spontaneous emission noise process.

In a first step at the receiver a Gaussian optical bandpass filter of 2nd order with a 3dB-bandwidth $\Delta B_{3dB} \sim 2R_b$ reduces the impact of the noise and

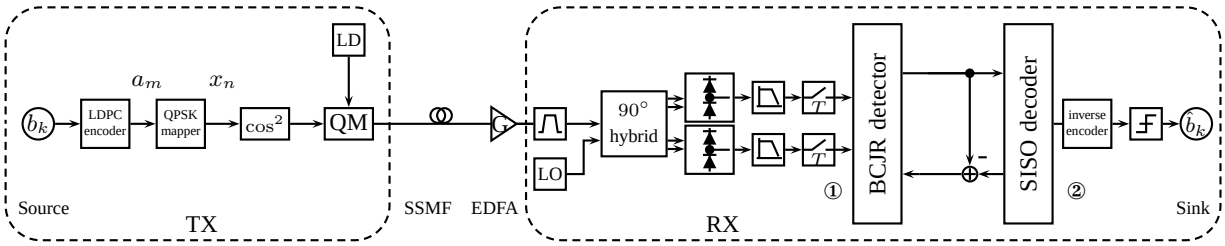


**Fig. 1**: Transmitter, fiber and receiver of coherent system with turbo equalization.

serves as a WDM demultiplexer. Then a 90° hybrid and two balanced photo diodes serve as an optical I-Q-demodulator, delivering the electrical inphase (I) and quadrature (Q) component of the demodulated QPSK signal. As the receiver electronics exhibit a lowpass characteristic, a 3rd order Bessel filter with 3dB-cut-off-frequency $f_{3dB} \sim 0.5R_b$ is inserted in the system to model this aspect. The electrical signal $q(t)$ is sampled at time instants $t = nT_s + t_0$. $T_s = 1/R_s$ is the interval of the QPSK symbols, and $n \in \mathbb{Z}$.

Finally the samples $q_n$ are handed to the turbo equalizer. It consists of a BCJR equalizer for detection and an iterative SISO LDPC decoder for error correction. The estimates $\hat{b}_k$ of the transmitted bit sequence $b_k$ are available after inverse encoding and hard decision of the decoded bitstream.

In the following the elements of the turbo equalizer are described in more detail.

# 3 Turbo Equalizer

## 3.1 BCJR Equalizer

The BCJR algorithm is a trellis based maximum a posteriori (MAP) symbol-by-symbol (sbs) estimation. The principal BCJR algorithm for binary phase shift keying (BPSK) modulated signals is well described in the literature [10], [11]. However, for higher order modulation like QPSK there are only few publications, e.g. [12] for mobile communications and 8-PSK modulation. Therefore we explain here, how to adapt the algorithm for QPSK modulation.

In principal, the BCJR algorithm is based on a trellis diagram. **Fig. 2** presents the trellis for a QPSK modulated signal and a channel memory of $\nu = 2$. It has $4^\nu = 16$ states and $4^{\nu+1} = 64$ state transitions. For each state, a forward metric $\tilde{\alpha}$ and a backward metric $\tilde{\beta}$ have to be calculated. They are recursively evaluated based on the branch metric $\tilde{\gamma}$ of each state transition.

For the turbo equalizer we use a Log-domain version of the BCJR algorithm, which is based on the Jacobian logarithm (JACLOG) [13]. Contrary to the probability domain BCJR algorithm it is a stable algorithm and reduces the computational complexity. The Jacobian logarithm is defined as

$$\begin{aligned} \mathrm{JacLog}\,(x,y) \doteq \max^*(x,y) \doteq \ln\left(e^x + e^y\right) = \\ = \max(x,y) + \ln\left(1 + e^{-|x-y|}\right). \end{aligned} \tag{2}$$

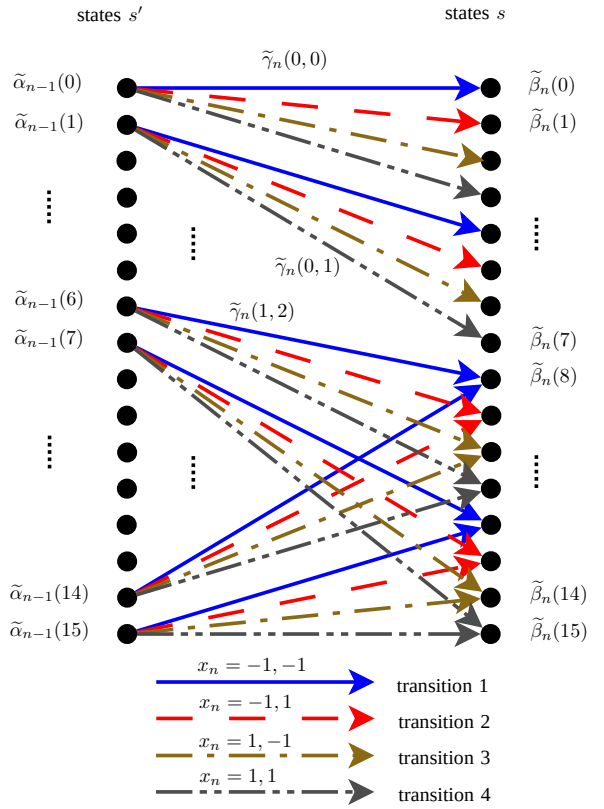


**Fig. 2**: Section of a trellis for QPSK modulated signal with channel memory $\nu = 2$.

The correction term $r(|x-y|) = \ln\left(1 + e^{-|x-y|}\right)$ is bounded ($0 < r(|x-y|) \leq \ln(2)$) and thus can be stored in a look-up table (LUT) [14], [15].

The computation of the forward metrics and backward metrics is the same as for BPSK modulated signals:

$$\tilde{\alpha}_n = \max^*\left[\tilde{\alpha}_{n-1} + \tilde{\gamma}_n(s', s)\right] \tag{3}$$

$$\tilde{\beta}_{n-1} = \max^*\left[\tilde{\beta}_n + \tilde{\gamma}_n(s', s)\right]. \tag{4}$$

However, for QPSK modulated signals the branch metric

$$\tilde{\gamma}_n(s', s) = \ln P\left[x_n\right] + \tilde{p}\left(q_n | x_n, s'\right) \tag{5}$$

contains the logarithm of the a priori probability (APP) $\ln\left(P\left[x_n\right]\right)$ of symbols (see section 3.2.1) and the logarithm (indicated by $\tilde{}$) of a two dimensional probability density function. The PDFs can efficiently be determined from collected histograms, which will be explained in section 3.2.2.

Finally, the extrinsic log-likelihood ratio (L-value) of each bit $x_{n,i}$ ($i = 1, 2$) of the symbol $x_n$ can be derived based on the metrics $\tilde{\alpha}$, $\tilde{\beta}$ and $\tilde{\gamma}^*$:

$$L\left(x_{n,i}\right) = \max_{U_i^+}{}^* \left(\tilde{\alpha}_{n-1}(s') + \tilde{\gamma}_n^*(s', s) + \tilde{\beta}_n(s)\right) - \max_{U_i^-}{}^* \left(\tilde{\alpha}_{n-1}(s') + \tilde{\gamma}_n^*(s', s) + \tilde{\beta}_n(s)\right), \quad (6)$$

where $\tilde{\gamma}_n^*(s', s)$ only contains the logarithm of the PDF and no a priori information. $U_i^+$ is the set of state transitions which corresponds to the event that bit $i$ of symbol $x_n$ is $+1$, $U_i^-$ is similarly defined. For the trellis of Fig. 2 the set of state transitions are

$U_1^+ = \{\text{state transitions 2 and 4}\}$
$U_1^- = \{\text{state transitions 1 and 3}\}$
$U_2^+ = \{\text{state transitions 3 and 4}\}$
$U_2^- = \{\text{state transitions 1 and 2}\}$.

## 3.2 Branch Metric Calculation

### 3.2.1 A-priori Information for the BCJR Algorithm

According to equ. (5) the branch metric contains the APP $P\left[x_n\right]$ of symbol $x_n$. This APP of a symbol can be rewritten as the joint probability of the unique bits $x_{n,i}$ of the symbol:

$$P\left[x_n\right] = P\left[x_{n,1}, x_{n,2}\right] = P\left[x_{n,1}|x_{n,2}\right] P\left[x_{n,2}\right] \quad (7)$$

Let us assume, the random variables representing both bits are statistically independent. Then $P\left[x_{n,1}|x_{n,2}\right] = P\left[x_{n,2}\right]$, thus the APP $P\left[x_n\right] = P\left[x_{n,1}\right] \cdot P\left[x_{n,2}\right]$ of the symbol is equal to the product of the probabilities of the bits. In equ. (5) of the branch metric, the a priori probability of the symbol can be written in the following way:

$$\tilde{\gamma}_n(s', s) = \ln P\left[x_{n,1}\right] + \ln P\left[x_{n,2}\right] + \tilde{p}\left(q_n|x_n, s'\right) \quad (8)$$

The feedback of the extrinsic a priori information of the decoder is not a probability but is given as an L-value. Thus, the probabilities of equ. (8) have to be expressed in terms of L-values. According to [5]

$$P\left[x_{n,i}\right] = \left(\frac{\exp\left(-\frac{1}{2}L(x_{n,i})\right)}{1 + \exp\left(-L(x_{n,i})\right)}\right) \exp\left(\frac{x_{n,i}}{2} L\left(x_{n,i}\right)\right) \quad (9)$$

with $i = 1, 2$ holds and for the logarithm

$$\ln P\left[x_{n,i}\right] = \underbrace{\ln\left(\frac{\exp\left(-\frac{1}{2}L(x_{n,i})\right)}{1 + \exp\left(-L(x_{n,i})\right)}\right)}_{\doteq A_{i,k}} + \frac{x_{n,i}}{2} L\left(x_{n,i}\right). \quad (10)$$

$A_{i,k}$ is a constant and is the same for all branch metrics. Thus it has no impact on the output of the BCJR and hence can be dropped. With equ. (10) and (8) the a priori information is considered in the branch metric as follows:

$$\tilde{\gamma}_n(s', s) = \frac{x_{n,1}}{2} L\left(x_{n,1}\right) + \frac{x_{n,2}}{2} L\left(x_{n,2}\right) + \tilde{p}\left(q_n|x_n, s'\right) \quad (11)$$

### 3.2.2 Efficient collection of the PDFs

Each branch of the trellis in Fig. 2 has its own PDF and is noted in the branch metric according to equ. (11). These PDFs can be determined from collected histograms. In our trellis with channel memory $\nu = 2$ and 16 states, in total 64 PDFs are required.

In [16] an experimental Viterbi equalizer was designed using 90 nm CMOS technology for binary modulation and a resolution of the incoming signal of 3 bit/sample. $2^{17} = 131072$ symbols are used to collect the histograms. This equalizer is designed for a 3 tap channel model with 2 memories. Consequently, the trellis exhibits $2^3 = 8$ state transitions. Thus, in average $2^{17}/2^3 = 2^{14} = 16384$ symbols are allotted to each histogram.

Our trellis in Fig. 2 exhibits 64 state transitions. If we want to spend the same average amount of symbols per histogram as for the experimental Viterbi equalizer, an eightfold amount of symbols are required. In case the channel memory is 4, there are 1024 state transitions and 1.677.216 symbols have to be taken into account to get the same average amount of symbols per histogram. The number is even higher, if the resolution of the incoming signal is larger than 3 bit. As we can see from these figures, for QPSK a huge memory is necessary to collect the histograms.

However, a much smaller amount of symbols is sufficient if only the mean and the variance of the PDFs are required. This is the case for the given optical system as the probability density functions can be approximated by a Gaussian function. Collecting $2^{16} = 65536$ symbols, it is possible to estimate the mean and the variance. Thus, complexity is reduced significantly.

## 3.3 Soft-In Soft-Out Decoder

An LDPC code is used since these codes can approach the capacity with low-complexity decoding. Furthermore, LDPC codes are suited for high code rates and thus are of interest for optical communications. LDPC codes are a subset of linear block codes and are specified by their parity check matrix $\mathbf{H}$. An example of such a parity check matrix is as

$$\mathbf{H} = \left[\begin{array}{ccccccc|ccccccc} 1 & 0 & 0 & 0 & 1 & 0 & 0 & 1 & 1 & 0 & 0 & 0 & 0 & 0 \\ 0 & 1 & 0 & 0 & 0 & 1 & 0 & 0 & 1 & 1 & 0 & 0 & 0 & 0 \\ 0 & 0 & 1 & 0 & 0 & 0 & 1 & 0 & 0 & 1 & 1 & 0 & 0 & 0 \\ 1 & 0 & 0 & 1 & 0 & 0 & 0 & 0 & 0 & 0 & 1 & 1 & 0 & 0 \\ 0 & 1 & 0 & 0 & 1 & 0 & 0 & 0 & 0 & 0 & 0 & 1 & 1 & 0 \\ 0 & 0 & 1 & 0 & 0 & 1 & 0 & 0 & 0 & 0 & 0 & 0 & 1 & 1 \\ 0 & 0 & 0 & 1 & 0 & 0 & 1 & 1 & 0 & 0 & 0 & 0 & 0 & 1 \end{array}\right]. \quad (12)$$

The codeword length, i.e. the number of columns of this parity check matrix is $N = 14$ and the number of rows is $J = 7$. Each row has $\rho = 4$ and each column has $\gamma = 2$ ones. This code is regular, as the number of ones per row and per column is constant. Usually, the density of ones is much smaller as in this example.

### 3.3.1 Sum-Product Algorithm

For LDPC decoding an iterative SISO decoder, the so called sum-product-algorithm (SPA) decoder [17] is used

to determine the sbs-MAP probability for each information bit. This decoder is based on the Tanner graph [18]. **Fig. 3** represents the Tanner graph for the parity check matrix of equ. (12) as an example.

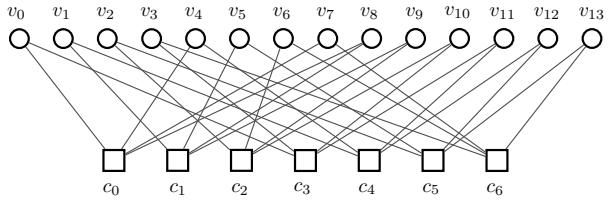


**Fig. 3**: Tanner graph for parity check matrix of equ. (12).

In each iteration information is passed between the variable node (VNP, $v_i$) and check node processors (CNP, $c_i$). In the first iteration, the variable nodes receive the extrinsic L-values from the BCJR equalizer and pass them to the check nodes in form of the channel value matrix $\mathbf{Z^{(i+1)}}$.

The calculation rule of the check node processor is

$$\epsilon_l\left(\vec{h}_j\right) = \left(\prod_{t\in B\left(\vec{h}_j\right)\backslash l} \alpha_{j,t}\right) \Phi\left(\sum_{t\in B\left(\vec{h}_j\right)\backslash l} \Phi\left(\beta_{j,t}\right)\right), \tag{13}$$

with

$$\Phi\left(x\right) = -\ln\tanh\left(\frac{1}{2}x\right), \tag{14}$$

$\alpha_{j,l} = \text{sign}\left(Z_{j,l}\right)$, $\beta_{j,l} = |Z_{j,l}|$ and $\vec{h}_j$ denotes the rows of the parity check matrix $\mathbf{H}$ ($j = 1...J$). $t \in B\left(\vec{h}_j\right)$ is the set of indices of ones in row $j$. Equ. (13) can be implemented by a CNP according to **Fig. 4**.

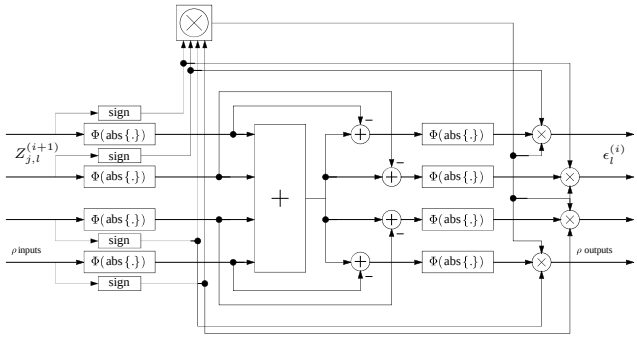


**Fig. 4**: Check node processor of SPA decoder for code with $\rho = 4$.

The VNP sums up the extrinsic information of the CNP and the channel information matrix $\mathbf{Y}$ which consists of the extrinsic L-values of the equalizer. Matrix $\mathbf{Y}$ has dimension $J \times N$. The channel value matrix for the next iteration step is

$$\mathbf{Z^{(i+1)}} = \mathbf{Y} + \mathbf{E^{(i)}}, \tag{15}$$

with

$$E_{j,l}^{(i)} = \sum_{\vec{h}_t\in A_l\backslash\vec{h}_j} \epsilon_l^{(i)}\left(\vec{h}_t\right), \quad \epsilon_l^{(i)} = E_{j,l}^{(i)} + \epsilon_l\left(\vec{h}_j\right) \tag{16}$$

The extrinsic matrix $\mathbf{E^{(i)}}$ and matrix $\mathbf{Y}$ exhibit elements unequal to zero at those positions where $\mathbf{H}$ has a one as entry.

Equ. (15) can be implemented in a VNP according to **Fig. 5**. At the end of the last decoder iteration the output L-values are available at the VNP.

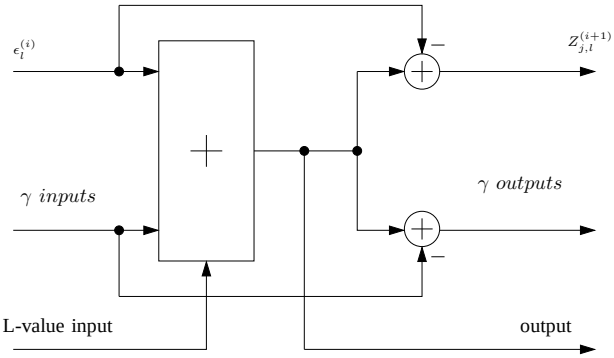


**Fig. 5**: Variable node processor of the SPA decoder for code with $\gamma = 2$.

### 3.3.2 Complexity of the Decoder

In this section a rough estimation of the decoder complexity will be given. The estimation holds for regular LDPC codes. In the next chapter, the complexity of the decoder will be an important aspect to select an appropriate LDPC code for the turbo equalizer.

The number of operations to be performed in the decoder depends on the number of CNPs and VNPs and the number of input signals of the nodes. The number of CNPs in a Tanner graph is $J$ and the number of VNPs is $N$. For a regular code, each check node processor exhibits $\rho$ inputs and each variable node processor has $\gamma$ inputs. **Tab. 1** specifies the number of operations of the decoder according to equ. (13) and (15) and in dependence of the wordlength $Q$ of the signals passed between VNP and CNP.

| operation | # inputs | # elements |
|---|---|---|
| variable node processor: | | |
| real addition | $(\gamma+1)\,Q$ | $1 \cdot N$ |
| real subtraction | $2 \cdot Q$ | $\gamma \cdot N$ |
| check node processor: | | |
| sign-operation | | $\rho \cdot J$ |
| magnitude | $Q$ | $2 \cdot \rho \cdot J$ |
| real addition | $\rho \cdot Q$ | $1 \cdot J$ |
| real subtraction | $2 \cdot Q$ | $\rho \cdot J$ |
| multiplication | | $1 \cdot J$ |
| multiplication | | $\rho \cdot J$ |
| $\Phi\left(x\right)$ | $Q$ | $2 \cdot \rho \cdot J$ |

**Table 1**: Operations of variable node and check node of the SPA decoder for estimation of complexity.

The implementation of the variable node processor is rather simple, as it only consists of adders. In the check node processors the function $\Phi\left(x\right)$ has to be executed. This operation is the most complex one of the decoder, because it goes beyond the elementary operations of the CNP which are just addition, subtraction and changing sign. Thus, the complexity of the decoder is mainly given

by $\Phi(x)$. It can be implemented as a look up table with complexity proportional to $2^Q$.

Assuming that for each $\Phi(x)$ an own LUT is implemented, the complexity of the decoder for a given LDPC code can be estimated by the product of $J\rho \cdot 2^{Q+1}$. The larger this product, the more complex the decoder. As a consequence, LDPC codes with a small row weight $\rho$ are advantageous with respect to implementation complexity of the decoder.

# 4 Simulation Results

## 4.1 Finite geometry LDPC Codes for coherent optical Receivers

There are many different ways to construct LDPC codes. We focus on regular codes based on Euclidian and projective geometries with code overhead between 5 and 15%. These codes enable encoding with simple shift registers, which is of benefit for high clock frequencies. They were recently developed and investigated for fiber optic communications [7], [9], [19]. By the use of techniques like code shortening and extension described in [9] a huge variety of codes have been obtained [20].

We have investigated the performance of the designed LDPC codes by computer simulations in order to find the most suitable ones for the turbo equalizer. **Tab. 2** presents a selection of codes for an overhead of 6.7%, 12.5% and 14.3%.

**Fig. 6** compares the bit error ratio (BER) vs. optical signal to noise ratio (OSNR) for all listed LDPC codes. The numerical analysis is based on the optical transmission scheme according to Fig. 1 with bit rate $R_b$ = 40 Gbit/s and a residual chromatic dispersion of $R_D$= 1063 ps/nm. The SPA decoder performs 25 iterations and over the turbo loop ten iterations are executed. For an overhead of 6.7% in particular code 1 has a good BER performance. Codes 3 and 4 are too short for this overhead and thus the turbo-cliff is not as steep as for code 1. Thus, a higher OSNR is required to reach the same bit error ratio. For an overhead of 12.5% code 7 has the best performance and for $O_c$ = 14.3% code 10 and 11 exhibit the best performance.

As argued in section 3.3.2, an estimation of the complexity of the SPA decoder for a given code is given by $J\rho \cdot 2^{Q+1}$. The wordlength $Q$ of the signals is not a property of the code. Consequently, for a relative comparison of the complexity of the decoders, the product $J\rho$ is sufficient, as given in Tab. 2. The figures prove that the decoder of code 1 exhibits the highest and of code 4 the lowest complexity. However, code 4 has a poor BER-performance. Codes 7, 10 and 11 have almost the same complexity as code 4 but better performance. With respect to the overhead, performance and complexity code 7 is the best compromise.

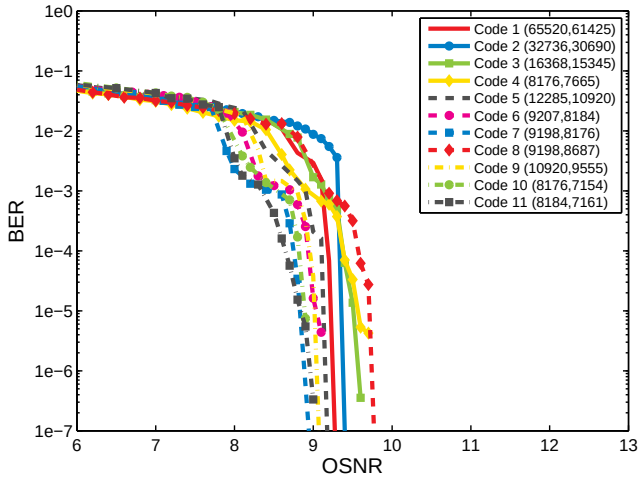


**Fig. 6**: BER vs. OSNR of the RX with turbo equalization for different LDPC codes, $R_D$ = 1063 ps/nm.

## 4.2 Comparison of Turbo Equalizer and FIR filter for CD Compensation

As outlined in [3], chromatic dispersion can also be compensated with FIR filters. Thus, we consider now the receiver in **Fig. 7** to compare its performance with the turbo equalizer.

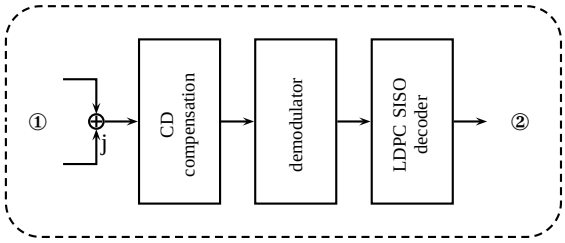


**Fig. 7**: Receiver with FIR filter for compensation of chromatic dispersion, the turbo equalizer between ① and ② in Fig. 1 is replaced by this part.

The BER of the receiver with FIR filter is plotted in **Fig. 8**. Codes 1,2, 7 and 10 exhibit a steep turbo cliff. As can be seen, some codes show a distinct error floor, which does not appear for the turbo receiver at BER $\geq 10^{-7}$.

The required OSNR at a BER of $10^{-7}$ as a function of the residual chromatic dispersion $R_D$ for both receivers is plotted in **Fig. 9** for codes 1, 7 and 10. For both systems code 10 requires the lowest OSNR, followed by code 7. For high $R_D$ a gain of up to 2.5 dB can be achieved with the turbo equalizer. Thus, for long haul transmission the turbo equalizer has superior performance.

## 4.3 Polarization Mode Dispersion

The receiver with the turbo equalizer is also capable to cope with differential group delay distortion due to PMD. First results of our investigation are depicted in **Fig. 10**. Here, the BER performance for code 1, 7 and 10 is plotted for $\Delta\tau$ = 100 ps.

| | $N$ | $K$ | $N-K$ | $R_c$ | $O_c$ | $c$ | $\rho$ | $\gamma$ | $J$ | $J \cdot \rho$ | $J \cdot \rho/24528$ |
|---|---|---|---|---|---|---|---|---|---|---|---|
| Code 1 | 65520 | 61425 | 4095 | 0.938 | 6.7% | 1 | 64 | 4 | 4095 | 262080 | 10.7 |
| Code 2 | 32736 | 30690 | 2046 | 0.938 | 6.7% | 32 | 63 | 4 | 2046 | 128898 | 5.3 |
| Code 3 | 16368 | 15345 | 1023 | 0.938 | 6.7% | 16 | 64 | 4 | 1023 | 64449 | 2.6 |
| Code 4 | 8176 | 7665 | 511 | 0.938 | 6.7% | 16 | 48 | 3 | 511 | 24528 | 1.0 |
| Code 5 | 12285 | 10920 | 1365 | 0.889 | 12.5% | 9 | 45 | 5 | 1365 | 61425 | 2.5 |
| Code 6 | 9207 | 8184 | 1023 | 0.889 | 12.5% | 9 | 36 | 4 | 1023 | 36828 | 1.5 |
| Code 7 | 9198 | 8176 | 1022 | 0.889 | 12.5% | 9 | 27 | 3 | 1022 | 27594 | 1.1 |
| Code 8 | 9198 | 8687 | 1022 | 0.889 | 12.5% | 9 | 72 | 3 | 1022 | 73584 | 3.0 |
| Code 9 | 10920 | 9555 | 1365 | 0.875 | 14.3% | 8 | 40 | 5 | 1023 | 40920 | 1.7 |
| Code 10 | 8176 | 7154 | 1022 | 0.875 | 14.3% | 8 | 32 | 4 | 1022 | 32704 | 1.3 |
| Code 11 | 8184 | 7161 | 1023 | 0.875 | 14.3% | 1 | 28 | 4 | 1023 | 28644 | 1.2 |

**Table 2**: Selected LDPC codes. $N$: codeword length, $K$: information word length, $R_c$: code rate $R_c = K/N$, $O_c$: code overhead $O_c = 1 - R_c^{-1}$, $c$: number of square matrices that compose the code, $\rho$: row weight, $\gamma$: column weight, $J$: number of rows in the parity check matrix.

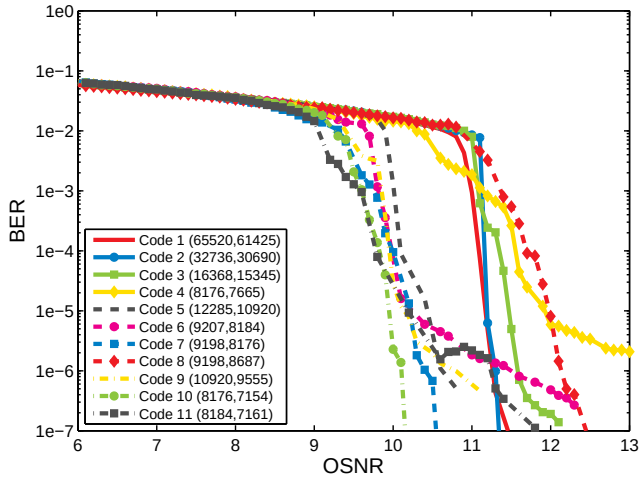


**Fig. 8**: BER vs. OSNR of the RX with FIR filter for CD compensation, $R_D$ = 1063 ps/nm.

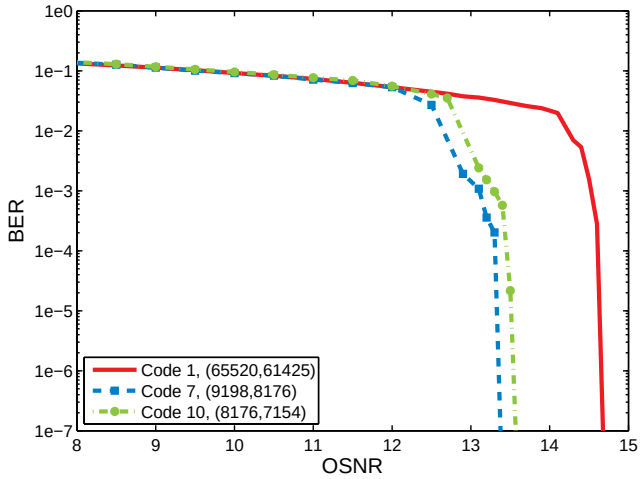


**Fig. 10**: BER vs. OSNR of the RX with turbo equalization for dedicated LDPC codes, $\Delta\tau$ = 100 ps, $R_D$ = 0 ps/nm.

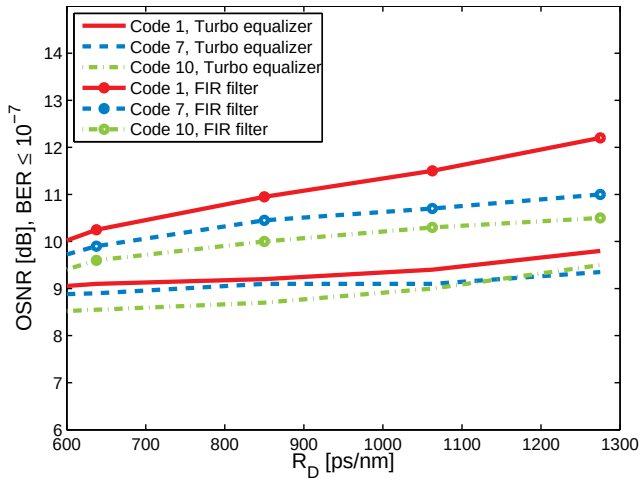


**Fig. 9**: Required OSNR versus residual chromatic dispersion $R_D$ for a receiver operating at BER of $10^{-7}$ and at $R_b$ = 40 Gbit/s for selected LDPC codes.

# 5 Conclusion

For coherent optical transmission, we have investigated a receiver with a turbo equalizer composed of a BCJR equalizer for electronic detection and an LDPC decoder. It has been shown in detail, how the BCJR equalizer can be adapted for QPSK modulated signals and how the log-likelihood ratios of symbols as a priori information for the equalizer can be found. A crucial point for equalization of higher order modulation is to get the probability density functions (PDFs) of the signal. For that purpose, a memory-efficient estimation of the PDFs has been proposed and used for the simulation of the system.

Finite geometry LDPC codes with overhead in the range of 6.7% up to 14.3% were presented. The BER performance of these codes and the complexity of the LDPC decoder has been compared. It has been shown, that decoders for powerful LDPC codes with overhead of 6.7% exhibit a high complexity. In contrast, for high performance codes with 12.5% and 14.3% overhead, the complexity is five to ten times smaller. We found out, that an LDPC code of codeword length 9198 and overhead

of 12.5% shows the best compromise between overhead, complexity of the decoder and the performance.

Further, we compared the performance of the receiver with turbo equalization to a receiver which compensates the chromatic dispersion by the use of a FIR filter on the basis of the same LDPC codes. As a result the receiver with the turbo equalizer has an OSNR gain of up to 2.5 dB at BER = $10^{-7}$ and high residual chromatic dispersion. Thus, the receiver with turbo equalization is well suited for long haul optical fiber links.

In future works, the performance of the turbo equalizer for a coherent system with polarization multiplex will be evaluated.

## Acknowledgement

This work was carried out in the framework of the project "Coding and equalization for coherent optical communication systems" and funded by Deutsche Forschungsgemeinschaft (DFG) which is gratefully acknowledged.

# References

[1] G. Charlet, "Coherent detection associated with digital signal processing for fiber optics communication," *Comptes Rendus Physique*, vol. 9, pp. 1012–1030, Nov. 2008.

[2] E. Ip, A. P. T. Lau, D. J. F. Barros, and J. M. Kahn, "Coherent detection in optical fiber systems," *Opt. Express 16*, pp. 753–791, 2008.

[3] S. J. Savory, "Digital filters for coherent optical receivers," *Opt. Express 16*, pp. 804–817, 2008.

[4] J. Renaudier, O. Bertran-Pardo, G. Charlet, M. Salsi, H. Mardoyan, P. Tran, and S. Bigo, "8 Tb/s long haul transmission over low dispersion fibers using 100 Gb/s PDM-QPSK channels paired with coherent detection," *Bell Labs Technical Journal*, vol. 14, no. 4, pp. 27–45, 2010.

[5] J. Hagenauer, "The turbo principle: Tutorial introduction and state of the art," *Proceedings of the International Symposium on Turbo Codes, Brest, France*, pp. 1–11, Sep. 1997.

[6] M. Tüchler, R. Koetter, and A. Singer, "Turbo equalization: Principles and new results," *IEEE Transactions on Communications*, vol. 50, pp. 754–767, May 2002.

[7] T. Rankl, "Performance and bounds of optical receivers with electronic detection and decoding," Dr.-Ing. dissertation (Ph.D), Institute of Telecommunications, University Stuttgart, Stuttgart, 2010.

[8] T. Rankl, C. Kurz, and J. Speidel, "Performance bounds of optical receivers with electronic detection and decoding," *J. Lightw. Technol.*, vol. 27, no. 16, pp. 3567–3579, Aug. 2009.

[9] K. Oestreich and J. Speidel, "Implementation requirements for Gbit/s optical receivers with turbo detection and LDPC decoding," *ITG Symposium on Photonic Networks, Leipzig*, May 2010.

[10] L. Bahl, J. Cocke, F. Jelinek, and J. Raviv, "Optimal decoding of linear codes for minimizing symbol error rate," *IEEE Trans. Inf. Theory*, vol. 20, pp. 284–287, Mar 1974.

[11] W. E. Ryan, *Wiley Encyclopedia of Telecommunications*. John Wiley and Sons, Aug. 2003, ch. Concatenated convolutional codes and iterative decoding.

[12] V. Franz and G. Bauch, "Turbo-detection for enhanced data for GSM evolution," in *IEEE ITS Vehicular Technology Conference (VTC)*, vol. 5, 1999, pp. 2954 –2958 vol.5.

[13] P. Robertson, E. Villebrun, and P. Hoeher, "A comparison of optimal and sub-optimal MAP decoding algorithms operating in the log domain," in *IEEE International Conference on Communications (ICC), Seattle*, vol. 2, Jun. 1995, pp. 1009–1013.

[14] S. ten Brink, "Design of concatenated coding schemes based on iterative decoding convergence," Dr.-Ing. dissertation (Ph.D), Institute of Telecommunications, University Stuttgart, Stuttgart, 2001.

[15] ——, "Convergence behaviour of iteratively decoded parallel concatenated codes," *IEEE Trans. Commun.*, vol. 49, no. 10, pp. 1727–1737, Oct. 2001.

[16] T. Veigel, M. Grözing, M. Berroth, and F. Buchali, "Design of a Viterbi equalizer circuit for data rates up to 43 Gb/s," in *ESSCIRC Fringe*, Sep. 2009.

[17] S. Lin, J. Daniel, and J. Costello, *Error control coding*. Prentice Hall, New York, 2005.

[18] R. G. Tanner, "A recursive approach to low complexity codes," *IEEE Trans. Inform. Theory*, Sep. 1981.

[19] H. Bülow and T. Rankl, "Soft decoded modulation for sensitivity enhancement of coherent 100-Gbit/s transmission systems," in *Conference on Optical Fiber Communications (OFC) - post deadline papers*, Mar. 2009, pp. 1–3, oFC.

[20] R. Rankl, M. Breuninger, and K. Oestreich, "Shortened finite geometry LDPC codes with 5 to 15 per cent code overhead for fiber optic communications," Aug. 2009, report Institute of Telecommunications, University of Stuttgart, Stuttgart. [Online]. Available: http://www.inue.uni-stuttgart.de/publications/pub_2009/rankl_internalReport_2009.pdf